THE JOURNAL OF PHYSICAL CHEMISTRY B

Article

pubs.acs.org/JPCB

NEXAFS Sensitivity to Bond Lengths in Complex Molecular Materials: A Study of Crystalline Saccharides

Adrian Gainar,[†] Joanna S. Stevens,[†] Cherno Jaye,[‡] Daniel A. Fischer,[‡] and Sven L. M. Schroeder*[,†,§,∥]

[†]School of Chemical Engineering and Analytical Science, The University of Manchester, Oxford Road, Manchester M13 9PL, United Kingdom

[‡]Material Measurement Laboratory, National Institute of Standards and Technology, Gaithersburg, Maryland 20899, United States

[§]School of Chemical and Process Engineering, University of Leeds, Leeds LS2 9JT, United Kingdom

[∥]DIAMOND Light Source Limited, Harwell Science and Innovation Campus, Chilton, Didcot OX11 0DE, United Kingdom

Supporting Information

ABSTRACT: Detailed analysis of the C K near-edge X-ray absorption fine structure (NEXAFS) spectra of a series of saccharides (fructose, xylose, glucose, galactose, maltose monohydrate, α-lactose monohydrate, anhydrous β-lactose, cellulose) indicates that the precise determination of IPs and σ^* shape resonance energies is sensitive enough to distinguish different crystalline saccharides through the variations in their average C−OH bond lengths. Experimental data as well as FEFF8 calculations confirm that bond length variations in the organic solid state of 10^{-2} Å can be experimentally detected, opening up the possibility to use NEXAFS for obtaining incisive structural information for molecular materials, including noncrystalline systems without long-range order such as dissolved species in solutions, colloids, melts, and similar amorphous phases. The observed bond length sensitivity is as good as that originally reported for gas-phase and adsorbed molecular species. NEXAFS-derived molecular structure data for the condensed phase may therefore be used to guide molecular modeling as well as to validate computationally derived structure models for such systems. Some results indicate further analytical value in that the σ^* shape resonance analysis may distinguish hemiketals from hemiacetals (i.e., derived from ketoses and aldoses) as well as α from β forms of otherwise identical saccharides.

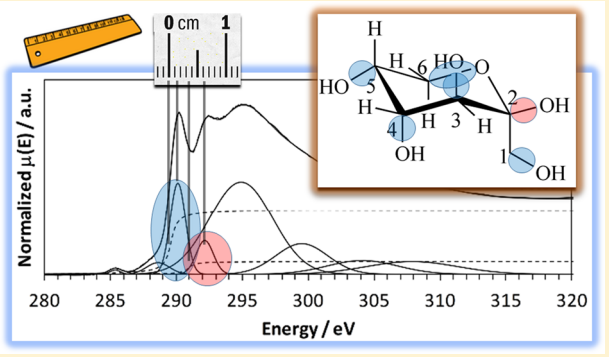

INTRODUCTION

Saccharides, also known as carbohydrates and sugars, are an important class of natural products and are well-known as foods and components of ingestible formulated products.[1−6] They have a propensity to present various noncrystalline and crystalline forms, and interest in intra- and intermolecular bonding in their solid state structures goes back to the earliest days of organic chemistry.[7] Saccharides can exist as monomers or, covalently bonded, as dimers, oligomers, or polymers, in which molecular monomers are linked by glycosidic bonds. Well-known monosaccharides are glucose (dextrose, also known as *blood sugar*), fructose (or *fruit sugar*), and ribose, an essential component of ribonucleic acid (RNA). Among disaccharides, well-known representatives are sucrose (*table/beet/cane sugar*, or simply *sugar*) and lactose (*milk sugar*), which is commonly used in pharmaceutical products as an excipient. The most abundant polysaccharide occurring in nature is cellulose,[8] which confers support, resistance, and rigidity to plants. In terms of classification by the number of carbons, saccharides with five carbon atoms in their molecules are called pentoses (e.g., ribose, xylose, lyxose), while six-membered ring saccharides are called hexoses (e.g., glucose, fructose, galactose).

Identifying mono-, di-, oligo-, and polysaccharides spectroscopically is often important for understanding the properties of formulated products.[9] X-ray core level spectroscopies are structurally incisive methods that are increasingly used for the analysis of interfacial species in complex products, devices, and biomaterials.[9−14] The most commonly used variant, X-ray photoelectron spectroscopy (XPS), provides information on the chemical state of atoms through sensitivity to the local electron density variations caused by changes in chemical bonding, which lead to chemical shifts of core level binding energies, and interpretation can be complemented or enhanced with the results of density functional theory (DFT) calculations.[15] Careful C 1s core level binding energy measurements by XPS of fructose, xylose, glucose, galactose, maltose, α-lactose, β-lactose, and cellulose have previously

Received: July 23, 2015
Revised: October 12, 2015
Published: October 12, 2015

DOI: 10.1021/acs.jpcb.5b07159
J. Phys. Chem. B 2015, 119, 14373−14381

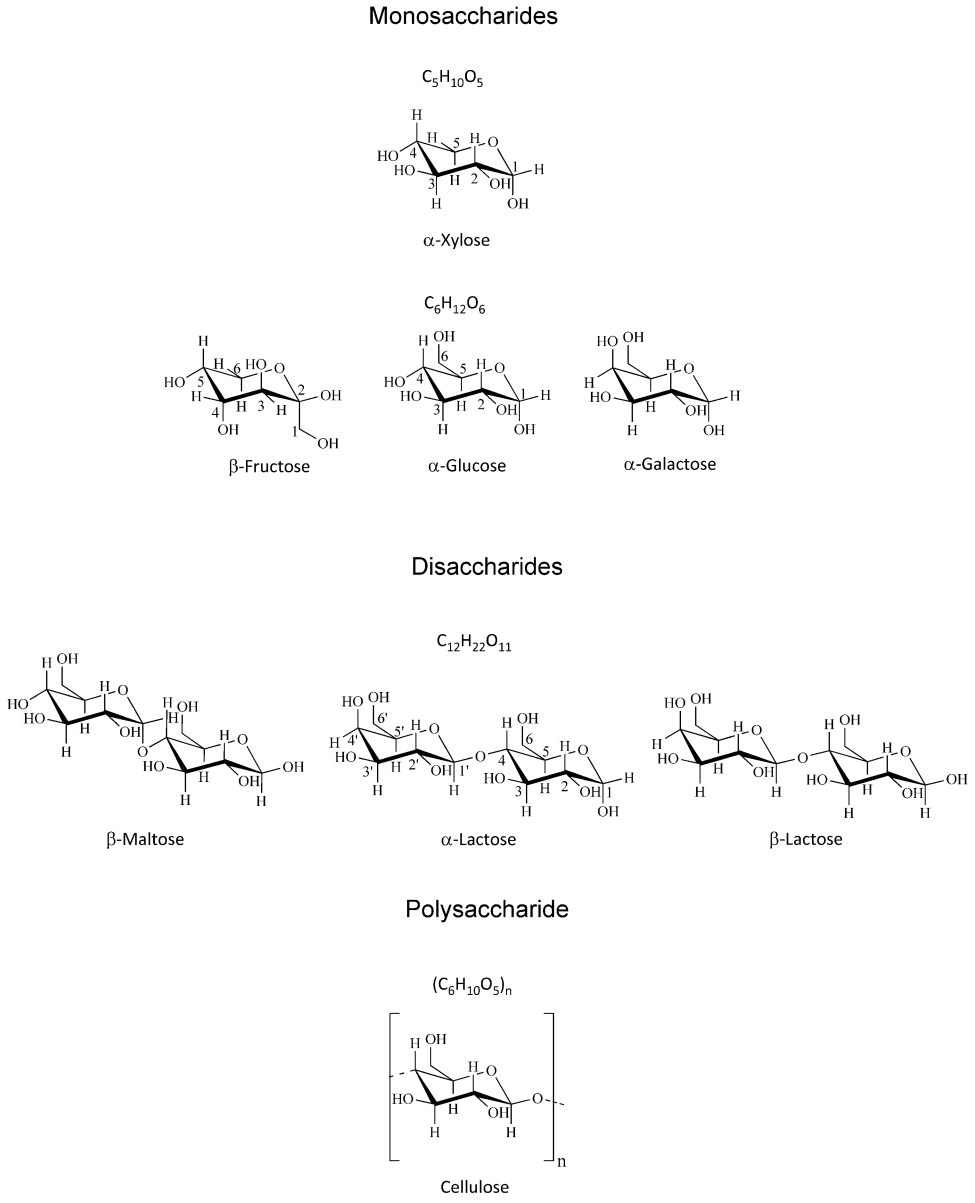

Figure 1. Saccharides analyzed by NEXAFS. IUPAC numbering of the carbon atoms is included for xylose, fructose, glucose, and α-lactose. Other mono- and disaccharides and the polysaccharide adopt analogous numbering.

revealed that XPS is sensitive enough to distinguish mono-, di-, and polysaccharides.[16]

Near-edge X-ray absorption fine structure (NEXAFS, also called X-ray absorption near-edge structure, XANES)[17] provides more incisive information than XPS about local chemical and electronic structure in condensed matter. Determination of bond lengths, static and dynamic disorder, as well as coordination numbers and coordination geometry around the X-ray absorbing atoms in organic compounds can sometimes also be achieved by extended X-ray absorption fine structure analysis (EXAFS).[17,18] However, C K-edge EXAFS analysis is often not possible because of reciprocal space limitations caused by (i) spectral overlap of absorption edges from other elements (for the present case of saccharides the O K-edge ~250 eV above the C K-edge) and (ii) instrumental limitations such as source transmission variations due to contamination on optics, abrupt variations in photon flux, or nonlinearities in I_0 monitoring. However, NEXAFS offers the possibility to obtain information about bond lengths in organic molecules through determination of σ^* shape resonance energies relative to the ionization potential of the core level from which excitation takes place. σ^* shape resonances arise because photoexcited core electrons can be temporarily trapped by a centrifugal potential barrier near the edge of the molecule, so electrons traverse the molecule multiple times before escaping from the molecular core by tunneling.[17,19−23] The use of shape resonance energy shifts for determining bond lengths has been referred to as the "bond length with a ruler" method.[17,20−22,24] The method relies on the determination of the core level binding energies (i.e., variations in the core level ionization potentials, IPs) from the absorption spectra and the energetic position of the σ^* shape resonances relative to the IP.[25] We recently reported evidence that this method can also be applied to C−N bonds of organic molecules in solution and in the organic solid state.[22] The likely reason for this transferability of a method originally developed for gas-phase

DOI: 10.1021/acs.jpcb.5b07159
J. Phys. Chem. B 2015, 119, 14373−14381

molecules is that intermolecular interactions in the organic condensed phase are much weaker than the internal covalent bonds in the molecules. While the exact physical origins of σ^* shape resonances, and thus the validity of their use for bond length determination, has been controversially discussed in the past,[25−30] there is considerable empirical evidence as well as theoretical support[30,31] for their interpretation as multiple scattering resonances dependent on the bond length.[23]

Full deconvolution and interpretation of all features in NEXAFS spectra can be a complex task, but our previous success in detecting differences between saccharides by core level binding energy analysis in XPS[16] led us to hypothesize that the structurally more incisive NEXAFS spectroscopy may also be sensitive to differences in structure and bonding in saccharide systems. Note that unlike diffraction methods, core level spectroscopies do not require long-range order and can therefore also be applied to noncrystalline forms. A deeper understanding of the core level spectra of the crystalline forms would therefore establish a basis for characterization of local interactions in materials without long-range order, such as melts, solutions, coatings, or nanocrystalline forms. Literature references describing applications of NEXAFS to saccharides have been rather sporadic[32−34] and generally did not relate the spectra to specific structural details.

In this paper we will discuss C K NEXAFS data of a series of monosaccharides (fructose, xylose, glucose, galactose), disaccharides (maltose monohydrate, α-lactose monohydrate, anhydrous β-lactose), and one polysaccharide (cellulose), with the aim to provide a database of spectral fingerprints and establish what level of structural detail is evident in these spectra. In particular, we show by reference to the crystal structures that the σ^* shape resonance analysis of the NEXAFS provides access to rather small variations in intramolecular C−OH bond lengths in the molecules.

EXPERIMENTAL SECTION

Polycrystalline powder samples were obtained from Sigma-Aldrich, UK. Fructose, xylose, galactose, maltose monohydrate, and cellulose have ≥99% purity. Glucose was 99.5% pure. α-Lactose monohydrate and β-lactose have been provided by Sanofi-Aventis (Alnwick, U.K.) and were the same samples examined in our previous XPS study.[14] All samples were used as provided. Thick layers of powder were spread onto sticky copper tape with a clean thin spatula, ensuring complete covering of the tape surface, and then pressed on mechanically to obtain a compact layer.

Figure 1 summarizes the chemical structures of the analyzed saccharides. The pentose (xylose) in the first row has the chemical formula $C_5H_{10}O_5$, the hexoses (fructose, glucose, galactose) in the second row have the general chemical formula $C_6H_{12}O_6$, and the disaccharides (maltose, α-lactose, β-lactose) in the third row have the general formula $C_{12}H_{22}O_{11}$. The polysaccharide (cellulose) in the fourth row is a polymer of β-glucose having the formula $[C_6H_{10}O_5]_n$.

Generally, monosaccharides crystallize in the pyranose form, i.e., as 6-membered rings; fructose can crystallize in either pyranose or furanose (5-membered ring) form; the pyranose form of fructose is usually obtained by industrial crystallization processes, whereas the furanose form occurs in natural products. Xylose is naturally found in pyranose form. For the disaccharides, maltose, α-lactose, and β-lactose are formed of two monosaccharide units in pyranose form. The polysaccharide, cellulose, is formed of linked glucose units in the pyranose form.

A Rigaku Miniflex XRPD instrument was used to determine the polymorphic form of each saccharide powder, taking diffraction patterns over a 2θ range from 5° to 40°, at a rate of 1°/min with a 0.02° step. The X-ray source (Cu K_α 1.5406 Å) operated with 30 kV voltage and 15 mA current. The experimental patterns were compared with calculated crystal structure patterns based on published crystal structures and are included in the Supporting Information (Figures S1−S8). Results indicated that the forms were β-fructose, α-xylose, α-glucose, α-galactose, β-maltose, α-lactose monohydrate, and anhydrous β-lactose. The positions of the broad features in the pattern of amorphous cellulose (Figure S8 in the Supporting Information) indicated that residual local order was determined by nuclei of the I_α polymorph of cellulose.

NEXAFS spectra were measured at the National Institute of Standards and Technology U7A beamline of the National Synchrotron Light Source (NSLS) at Brookhaven National Laboratory (BNL) in New York, United States. Partial electron yield (PEY) C K-edge spectra were obtained using a channeltron electron multiplier with the sample positioned at the magic angle (54.7°) relative to the incident beam, with a photon flux of approximately 5×10^{10} photons/s. An entrance grid bias of −150 V was used for the C K-edge in the case of galactose and −50 V for the rest of the saccharides.

At −50 V grid bias the detected electron-yield signal is essentially the total Auger yield, i.e., the probing depth of the electron-yield signal is determined by the escape depth of all C KLL Auger electrons, including the whole background of inelastically scattered electrons on the low-energy side of the Auger emission lines,[35−38] which probes deeper than the elastic Auger or photoemission peaks. A previous experimental determination of the C K-edge probing depth in polymers yielded a value of ∼2 nm,[39] while experiments with signal attenuation in Cr metal indicate for photons at the C K-edge that the maximum probing depth is approximately 3.5 nm.[40] These values are equivalent to probing a few molecular layers deep into the saccharide materials and should hence confer bulk sensitivity. In line with this, our previous XPS analysis of the same saccharide materials through C 1s emission with an Al Kα source, which is associated with signal attenuation lengths only slightly higher (∼3 nm),[41] yielded chemical compositions consistent with those expected from the saccharide stoichiometries. Moreover, for molecular materials surface effects on internal bond lengths should be negligible, as intermolecular interactions in organic molecular solids are weak relative to the strength of the internal bonds in the molecules. The strongest intermolecular interaction in the saccharide bulk is hydrogen bonding. It is therefore expected that the C−O bond lengths derived from the bulk crystal structures used for the interpretation of our data are good models.

A toroidal spherical grating monochromator with 600 lines mm^{-1} grating was used to acquire the C K-edge data, yielding an energy resolution of approximately 0.1 eV. After collection, the spectra were normalized by the simultaneously recorded drain current from an in situ gold-coated, 90% transmission grid (I_0) which is situated in the X-ray beam path, to eliminate the incident beam intensity fluctuations and absorption features in the beamline optics. The monochromator energy scale calibration was performed through the 285.1 eV π^* graphite absorption by a carbon mesh located further upstream of I_0 (I_0_up). All spectra were processed using standard pre- and

DOI: 10.1021/acs.jpcb.5b07159
J. Phys. Chem. B 2015, 119, 14373−14381

postedge normalization methods. The peak-fitting capability of Athena software[42,43] was employed to determine the energetic positions of all NEXAFS transitions at the C K-edge, and the spectrum was modeled with Gaussians for the peaks and two arctan step functions for the edge steps arising at the IPs.[17] The positions of the IPs were determined assuming two constraints: the expected intensity ratio for OC−OH and C−OH moieties and their energy difference, which was known from our previous XPS study to be 1.35 eV higher for the OC−OH hemiacetal/hemiketal groups.[16] The first IP was set as the experimental edge step inflection point, i.e., the zero crossing of the second derivative of the experimental spectrum. For investigating the "bond length with a ruler" correlation, the standard deviation for the C−OH bond lengths in the reported crystal structures was ≤0.007 Å.[44−49] For the curve-fitted C K-edge spectra, by fitting with different models (variation of peak positions, functions, and the number of included peak functions) and using different initial values for the peak parameters we found that the error in energy positions for comparably good final fits was ≤0.02 eV.

Slightly varying levels of adventitious surface contamination were previously observed in the XPS data for the same set of saccharides.[16] In the NEXAFS spectra this contamination is evident as weak pre-edge peaks in the C K-edge spectra. Similar to the constant peak position of the hydrocarbon contaminant in XPS C 1s results,[16] these pre-edge peaks were in a narrow energy range, from 285.3 to 285.4 eV. We carefully checked by examination of the signal from the incident beam monitor (a gold coated mesh) whether varying levels of surface contamination on it might have led to normalization errors that could account for these pre-edge features. However, no variations in the mesh signal were evident that could cause the observed signals.

In the previous XPS analysis of saccharides, it was also noted that the intensity of the peaks from the C−OH and O−C−O hemiacetal/hemiketal moieties in the C 1s spectra decreased as a function of X-ray exposure[16] due to radiative damage, with the strongest effect on ribose and xylose.[16] In the NEXAFS measurements, no significant changes in peak positions and intensities nor formation of new peaks were observed as a function of exposure to the X-ray beam, even after six scans of the C K-edge.

FEFF8.2[50] was used to simulate the σ* shape resonances in the C K NEXAFS for a cluster cut from the crystal structure of glucose (CCDC reference: GLUCSA03).[51] The XANES, FMS, and SCF cards were used—FMS for full-multiple scattering X-ray absorption near-edge structure (XANES) calculation; SCF to enable self-consistent field iterations. To identify the shape resonance contributions due to scattering near the potential of the C−OH single bonds we also ran calculations in which the C−OH bond length in the hemiacetal/hemiketal position was increased and decreased by 0.1 Å relative to the equilibrium value in the crystal structure (see Figure 2 and Supporting Information).

RESULTS AND DISCUSSION

The C K NEXAFS spectra of the saccharides are presented in Figures 2 and 3 together with the results of the fitting analysis involving Gaussian and edge step functions. For a deeper analysis of these spectra we need to recall that saccharide molecules present only single C−C, C−H, and C−O bonds (Figure 1), so it is expected that the NEXAFS spectra are dominated by transitions to unoccupied, antibonding σ* states.

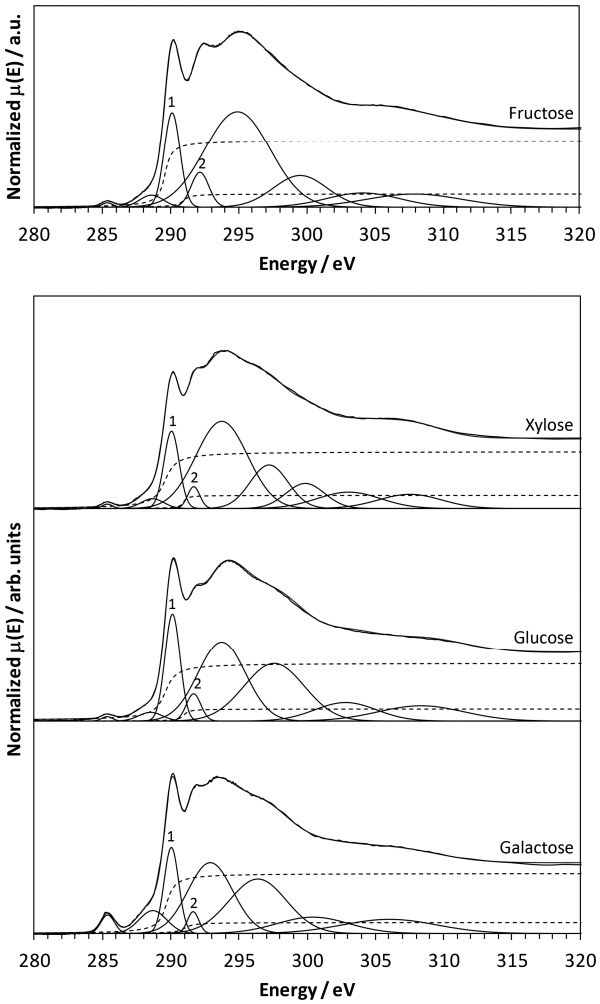

Figure 2. Experimental C K-edge spectrum of fructose (top plot) and C K-edge spectra (bottom plot) for the monosaccharides xylose (top), glucose (middle), and galactose (bottom). Each spectrum is accompanied by best fits obtained to determine peak positions, with the $\sigma^*_{\underline{C}-OH}$ and $\sigma^*_{O\underline{C}-OH}$ peaks marked by numbers 1 and 2, respectively. IP edge steps are marked with dashed lines.

The most prominent features are σ* shape resonances, which arise from multiple scattering of the photoelectron wave along the internuclear axis between the absorbing atom and its neighbor; thus, the σ* shape resonance energies depend sensitively on the associated intramolecular bond lengths.

In a previous study of the C K-edge spectra of a dimannoside derivative adsorbed on Au, the prominent σ* resonance at ∼289 eV was attributed to the C−OH moieties of the saccharide and the feature at ∼291 eV to the OC−OH moiety.[34] In line with this assignment, the intensity of peak 1 is reduced for xylose (Figure 2) as there is one less contributing carbon (i.e., one less C−OH bond in the structure), so the relative intensities of the peaks arising from the two moieties are different compared to the other monosaccharides. The small pre-edge peak at ∼285 eV in the spectra can be attributed to adventitious contamination with unsaturated hydrocarbons containing C═C bonds,[34] while the second pre-edge peak at ∼288 eV, observed as a shoulder, is associated with C−H transitions.[33] The broader features at higher photon energies around 294 eV may arise from C−C bonds.

To examine how the σ* transitions associated with C−OH bonds vary in energetic position as a function of bond length,

DOI: 10.1021/acs.jpcb.5b07159
J. Phys. Chem. B 2015, 119, 14373−14381

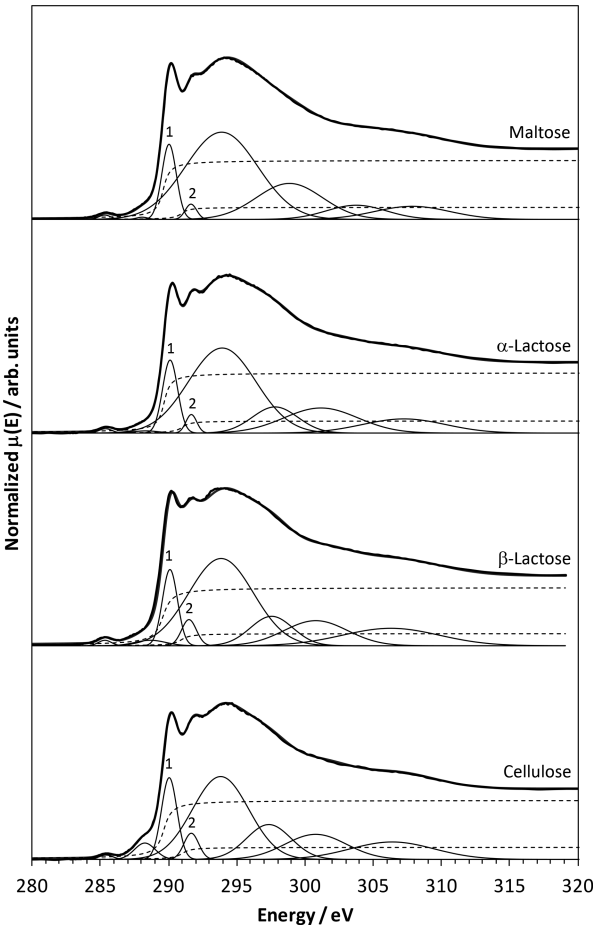

Figure 3. Experimental C K-edge spectra for the di- and polysaccharides studied, maltose (top), α-lactose (second from top), β-lactose (third from top), and cellulose (bottom), alongside fits with the $\sigma^*_{\underline{C}-OH}$ and $\sigma^*_{O\underline{C}-OH}$ peaks marked by numbers 1 and 2, respectively. IP edge steps are marked with dashed lines.

FEFF8 calculations were performed on each inequivalent C atom in the crystal structure of glucose, first with the equilibrium C−OH bond length in the crystal structure and then for the same bond shortened and elongated by 0.1 Å. One set of resulting spectra is presented in Figure 4 and the others in Figures S9−S13 of the Supporting Information. The strong shifts of the shape resonances originally in the region around 290−292 eV are evident, with a shorter bond length resulting in a blue shift (higher photon energy) by approximately +4.7 eV, whereas the longer bond length results in a red shift (lower photon energy) by about −4.2 eV.

As mentioned above, during peak fitting of the spectra in Figures 2 and 3, a 1.35 eV difference in energy between the IPs arising from C−OH and OC−OH moieties was assumed, as this is (with a margin of about ±0.05 eV) the value of the C 1s binding energy separations observed by XPS.[16] The intensity ratios between the two edge step functions representing the IPs were fixed to be in line with the stoichiometries of the saccharides.[16] Note that in the extended X-ray absorption fine structure (EXAFS) region at higher photon energies, where the spectra are determined by scattering of the photoelectron wave by neighboring atoms, the fitted Gaussian functions have no physical meaning, but modeling of the postedge background was required to ensure accurate fitting results in the spectral regions of the electronic transitions of interest, i.e., around and

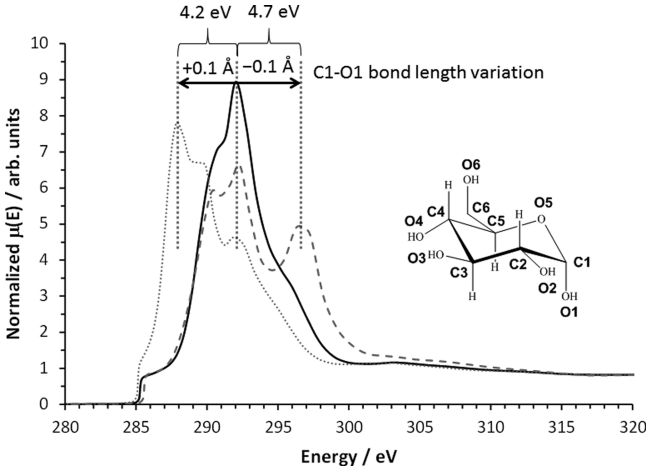

Figure 4. FEFF8 simulations for C1 absorbing atom in an unaltered crystal structure of glucose (black line), an altered crystal structure of glucose with the C1−O1 bond shortened by 0.1 Å (dashed gray line), and an altered crystal structure of glucose with the C1−O1 bond elongated by 0.1 Å (dotted gray line).

below the IPs. The parameters derived with the fitting results (shown in Figures 2 and 3) are summarized in Table 1. It can be seen that the $\sigma^*_{\underline{C}-OH}$ transitions are in a narrow range of energies, from 290.0 to 290.1 eV. The $\sigma^*_{O\underline{C}-OH}$ transitions are found between 291.5 and 292.1 eV.

We can now turn to examining how the crystallographically determined C−OH bond lengths correlate with the shifts in the σ^* shape resonances and IPs. This "bond length with a ruler" analysis[17,20−22] consists of plotting the term value δ, which is the energy difference between the σ^* shape resonance energy and its corresponding IP (Table 1), as a function of the length of the bond from which it arises. Because of the significant IP difference between the C−OH and the OC−OH moieties in the saccharides, their shape resonances are distinct, and their bond lengths can be determined separately. There are of course several C−OH moieties with slightly different bond lengths in each saccharide, so we used their average bond length for the analysis (Table 2), as available from their published crystal structures.[44−49,52,53] The OC−OH hemiacetal or hemiketal groups are associated with a shorter C−OH bond length (Table 2) than for the other C−OH groups,[44−49,52,53] and averaging of two values has to be used in the cases of the disaccharides and for cellulose, which is composed of repetitive interconnected motifs of two distinct cyclic glucose units bound by a glycosidic bond (i.e., cellulose can also be regarded as a polymer of a disaccharide). For the monosaccharides no averaging was required as there are no inequivalent OC−OH groups in the crystal structures. We also point out that contributions from the rather short endocyclic C−O bonds of the hemiacetal and hemiketal groups were omitted from bond length averaging as they are located in the energy region beyond 293 eV, where their contribution cannot be distinguished against the strong background arising from the C−C bonds. The other endocyclic C−O bond is always similar in length to the C−OH bonds and was therefore included in their average.

The resulting plot of the δ values as a function of the bond lengths is shown in Figure 5. It is evident that apart from two outliers (the OC−OH groups in β-lactose and fructose; see discussion below) there is a good linear correlation despite the small range (~0.05 Å) of bond length variations covered

DOI: 10.1021/acs.jpcb.5b07159
J. Phys. Chem. B 2015, 119, 14373−14381

Table 1. IPs and Centroid Energies of the σ^* Shape Resonances Determined by Curve Fitting[a]

saccharide	IP_{C-OH} (eV)	σ^*_{C-OH} (eV)	δ_{C-O} ($\sigma^*_{C-OH} - IP_{C-OH}$) (eV)	IP_{OC-OH} (eV)	σ^*_{OC-OH} (eV)	δ_{O-C-O} ($\sigma^*_{OC-OH} - IP_{OC-OH}$) (eV)
β-fructose	289.55	290.07	0.52	290.90	292.11	1.21
α-xylose	289.55	290.02	0.47	290.90	291.65	0.75
α-glucose	289.60	290.11	0.51	290.95	291.66	0.71
α-galactose	289.70	290.06	0.36	291.05	291.65	0.60
β-maltose monohydrate	289.55	289.98	0.43	290.90	291.58	0.68
α-lactose monohydrate	289.62	290.06	0.44	290.97	291.61	0.65
β-lactose	289.63	290.14	0.51	290.98	291.53	0.55
cellulose	289.60	289.99	0.39	290.95	291.61	0.66

[a]Term values δ are calculated as the difference between each σ^* centroid energy and its corresponding IP.

Table 2. C−OH Bond Lengths Determined by Crystal Structure Analysis[a]

saccharide	CSD identifier	C−OH bond length at OC−OH (1) (Å)	average length of remaining C−OH (av) (Å)
β-fructose	FRUCTO11[44]	1.412	1.423
α-xylose	XYLOSE[47]	1.393	1.424
α-glucose	GLUCSA03[45]	1.391	1.428
α-galactose	ADGALA01[46]	1.409	1.437
β-maltose monohydrate	MALTOS11[48]	1.402	1.418
α-lactose monohydrate	LACTOS03[49]	1.390	1.425
β-lactose	BLACTO02[53]	1.381	1.423
cellulose	PADTUL[52]	1.403	1.427

[a](1) represents the C−OH bond length from the hemiacetal or hemiketal group (as in Figure 1), and (av) represents the average values of the other the C−OH bond lengths (including one endocyclic C−O bond, see main text).

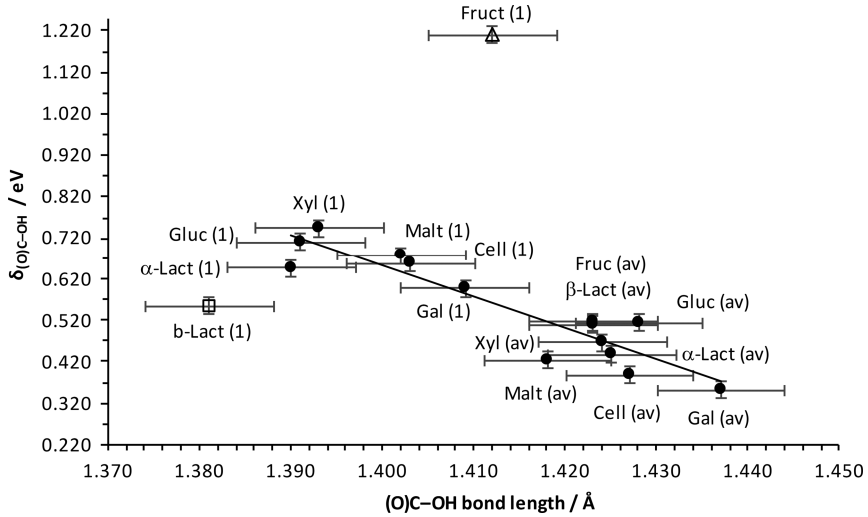

Figure 5. Linear correlation between term value δ and (O)C−OH bond length for the crystal structures of saccharides, where Fruct = fructose, Xyl = xylose, Gluc = glucose, Gal = galactose, Malt = maltose, α-Lact = α-lactose, β-Lact = β-lactose, Cell = cellulose; annotation (1) refers to the OC−OH bond length at the hemiacetal/hemiketal position (as in Figure 1), and (av) refers to the average value of the remaining C−OH bond lengths; fructose and β-lactose, outliers away from the fitted line (see discussion in the text), are represented with an empty triangle and an empty square, respectively.

(Figure 5). More precisely, for a change in the C−OH bond length by 0.047 Å, a term value shift of 0.393 eV occurs. Assuming that the term values can be determined with an accuracy of approximately 0.05 eV this suggests a sensitivity of the method to bond length variations slightly better than ∼0.01 Å, making the precision of the technique comparable to accuracies achievable by standard X-ray crystal structure determination. We note that these experimentally derived figures are also in good agreement with the C−OH shape resonance shifts predicted by the FEFF8 calculations (vide supra), which similarly indicated shifts of approximately 4.5 eV per 0.1 Å variation in bond length.

Turning to the outliers in the plot in Figure 5, for fructose the C−OH bond at the OC−OH group is considerably longer (1.412 Å) by comparison with the other saccharides (range 1.389−1.409 Å). The associated term value is also higher than that for the other saccharides. Both deviations are likely due to the fact that the OC−OH group in fructose represents a hemiketal rather than a hemiacetal moiety. As a result there is an additional C−C (rather than C−H) bond at the OC−OH moiety.[54] Interestingly, this result suggests that the NEXAFS analysis of C−OH σ^* shape resonances and IPs provides an avenue to distinguishing hemiketals from hemiacetals (i.e., ketoses from aldoses). However, more systematic work should

DOI: 10.1021/acs.jpcb.5b07159
J. Phys. Chem. B 2015, 119, 14373−14381

be carried out to confirm whether this observation can be generalized.

β-Lactose, the other outlier in Figure 5, has a significantly shorter C−OH bond at the OC−OH group than the other saccharides. It is distinguished from the other hemiacetals by a different configuration at the anomeric position, in which the OH group is positioned cis (rather than trans) to the $-CH_2OH$ group in the molecule. Moreover, unlike the other two disaccharides (β-maltose and α-lactose), the two monosaccharide units in the β-lactose structure are rotated relative to each other around the glycosidic bond. These local structure differences may perhaps combine to cause weak electronic structure variations and hence, e.g., slight differences in core hole relaxation or local screening differences that may affect the term value δ. A deeper analysis of other saccharide structures would be required to confirm or refute these points.

In any case, the outliers appear to underline an important constraint of the bond length with a ruler methodology, namely, that variations in the term value δ can only be compared for bonds in which the two atoms are in a similar chemical state, so additional dependencies on functional group identity (as in, aldehyde vs ketone) and (in condensed matter) secondary interactions with other functional groups due to conformational differences, configurational isomerism, and/or functional group interactions in the crystal structure may influence the results.

We investigated the possibility to additionally determine term values in the O K NEXAFS spectra, but the determination and interpretation of these values is more complex than for the C K-edge due to the additional influence of intermolecular hydrogen bonding, so that no firm conclusions could be drawn. Overall, however, the C K-edge results we obtained indicate that for hemiacetals with α configuration at the anomeric center the small relative energy variations between IPs and shape resonance features in the C K NEXAFS are, within experimental error, consistent with the variations of the C−O bond lengths known from single-crystal structure analysis. Our data lead to an estimate of a sensitivity to bond length variations on the order of ∼0.01 Å, which is in very good agreement with the previously reported sensitivity for gas-phase molecules.[21] Moreover, FEFF8 analysis confirms that the observed experimental energy shifts of the shape resonances are consistent with theoretical expectations for saccharides. These results suggest that careful use of solid state NEXAFS can provide very incisive structure information for molecular materials and should perhaps be considered more for the characterization of local bonding in noncrystalline systems, not only dissolved species as in a recent study[22] but also colloidal systems as well as melts and similar amorphous phases.

CONCLUSIONS

Analysis of the C K NEXAFS spectra of solid monosaccharides, disaccharides, and a polysaccharide indicates that the precise determination of IPs and σ^* shape resonance energies is sensitive enough to distinguish between different saccharides through the minute variations in C−O bond lengths in these systems. The analysis of the experimental data as well as FEFF8 calculations show that this sensitivity arises because bond length variations of 10^{-1} Å are associated with term value shifts on the order of ±4.5 eV, permitting determination of bond length variations of ∼0.01 Å. These observations suggest that NEXAFS can be used to obtain valuable bond length information for other molecular materials of similar complexity. Very importantly, NEXAFS is known to be applicable to noncrystalline systems (e.g., species in solutions, melts, amorphous phases, and adsorbed species), opening up an avenue toward structural information that can be used to confront computationally derived models for systems without long-range order. Moreover, the C K-edges of fructose and β-lactose do not fit into the trend set up by the other saccharides, suggesting that NEXAFS may also be sensitive enough to distinguish hemiketals from hemiacetals as well as α and β forms of the otherwise identical saccharides, but more systematic experimental work should examine these hypotheses.

ASSOCIATED CONTENT

Supporting Information

The Supporting Information is available free of charge on the ACS Publications website at DOI: 10.1021/acs.jpcb.5b07159.

X-ray powder diffraction patterns for each saccharide compared to calculated crystal structure patterns; results of FEFF8 calculations for each C atom in glucose with equilibrium, elongated and shortened C−O bond lengths (PDF)

Raw NEXAFS data files (ZIP)

Athena project file with fitted NEXAFS spectra (ZIP)

AUTHOR INFORMATION

Corresponding Author

*Phone/Fax: +44 (0)113 343 2401/2384. E-mail: s.l.m.schroeder@leeds.ac.uk.

Notes

The authors declare no competing financial interest.

ACKNOWLEDGMENTS

All data supporting this study are provided either in the results section of this paper or in the supplementary information accompanying it. We gratefully acknowledge support for A.G., J.S.S., and S.L.M.S. through an EPSRC Critical Mass Grant (EP/1013563/1). Use of the National Synchrotron Light Source, Brookhaven National Laboratory, was supported by the U.S. Department of Energy, Office of Science, Office of Basic Energy Sciences, under Contract No. DE-AC02-98CH10886. Commercial names mentioned in this manuscript are for illustrative purposes and do not represent an endorsement by the National Institute of Standards and Technology. S.L.M.S. holds the Bragg Centenary Chair at the University of Leeds, which is supported by the Royal Academy of Engineering, Diamond Light Source Ltd and Infineum UK, Ltd.

REFERENCES

(1) Rowe, R. C.; Sheskey, P. J.; Owen, S. C. *Handbook of Pharmaceutical Excipients*; Pharmaceutical Press and American Pharmacists Association: London and Washington, D.C., 2005.

(2) Holsinger, V. *Fundamentals of Dairy Chemistry*, 3rd ed.; Springer: Berlin, Heidelberg, New York, 1999.

(3) Johnson, D. C.; Lacourse, W. R. *Carbohydrate Analysis*; Elsevier: Amsterdam, 1995.

(4) Collins, P.; Ferrier, R. *Monosaccharides*; John Wiley & Sons: Chichester, 1995.

(5) Chaplin, M. F. *Carbohydrate Analysis-A Practical Approach*; Oxford University Press: Oxford, 1994.

(6) Lindhorst, T. K. *Essentials of Carbohydrate Chemistry and Biochemistry*; Wiley-VCH: Weinheim, 2007.

DOI: 10.1021/acs.jpcb.5b07159
J. Phys. Chem. B 2015, 119, 14373−14381

(7) Brown, G. M.; Levy, H. A. Alpha-D-Glucose - Determination of Crystal and Molecular Structure by Neutron-Diffraction Analysis. *Science* **1965**, *147*, 1038.
(8) Colvin, J. R. *The Biochemistry of Plants*; Academic Press: New York, 1980.
(9) Murrieta-Pazos, I.; Gaiani, C.; Galet, L.; Calvet, R.; Cuq, B.; Scher, J. Food Powders: Surface and Form Characterization Revisited. *J. Food Eng.* **2012**, *112*, 1−21.
(10) Kaivosoja, E.; Virtanen, S.; Rautemaa, R.; Lappalainen, R.; Konttinen, Y. Spectroscopy in the Analysis of Bacterial and Eukaryotic Cell Footprints on Implant Surfaces. *Eur. Cell Mater.* **2012**, *24*, 60−73.
(11) Benetti, F.; Marchettini, N.; Atrei, A. ToF-SIMS and XPS Study of Ancient Papers. *Appl. Surf. Sci.* **2011**, *257*, 2142−2147.
(12) Dietrich, P. M.; Horlacher, T.; Girard-Lauriault, P. L.; Gross, Th. s.; Lippitz, A.; Min, H.; Wirth, Th.; Castelli, R.; Seeberger, P.; Unger, W. E. Multimethod Chemical Characterization of Carbohydrate-Functionalized Surfaces. *J. Carbohydr. Chem.* **2011**, *30*, 361−372.
(13) Dietrich, P. M.; Horlacher, T.; Gross, Th.; Wirth, Th.; Castelli, R.; Shard, A. G.; Alexander, M.; Seeberger, P. H.; Unger, W. E. Surface Analytical Characterization of Carbohydrate Microarrays. *Surf. Interface Anal.* **2010**, *42*, 1188−1192.
(14) Willneff, E. A.; Ormsby, B. A.; Stevens, J. S.; Jaye, Ch.; Fischer, D. A.; Schroeder, S. L. M. Conservation of Artists' Acrylic Emulsion Paints: XPS, NEXAFS and ATR FTIR Studies of Wet Cleaning Methods. *Surf. Interface Anal.* **2014**, *46*, 776−780.
(15) Stevens, J. S.; Seabourne, C. R.; Jaye, Ch.; Fischer, D. A.; Scott, A. J.; Schroeder, S. L. M. Incisive Probing of Intermolecular Interactions in Molecular Crystals: Core Level Spectroscopy Combined with Density Functional Theory. *J. Phys. Chem. B* **2014**, *118*, 12121−12129.
(16) Stevens, J. S.; Schroeder, S. L. M. XPS Analysis of Saccharides and Their X-ray Induced Degradation. *Surf. Interface Anal.* **2009**, *41*, 453−462.
(17) Stöhr, J. *NEXAFS Spectroscopy*; Springer Series in Surface Sciences 25; Springer: Berlin, Heidelberg, 1992.
(18) Yang, B. X.; Kirz, J.; Sham, T. K. Oxygen K-Edge Extended X-ray Absorption Fine Structure Studies of Molecules Containing Oxygen and Carbon Atoms. *Phys. Rev. A: At., Mol., Opt. Phys.* **1987**, *36*, 4298−4310.
(19) *Atomic, Molecular and Optical Physics*; National Academic Press (National Research Council): Washington, D.C., 1986.
(20) Sette, F.; Stöhr, J.; Hitchcock, A. P. Determination of Intramolecular Bond Lengths in Gas-Phase Molecules from K-Shell Shape Resonances. *J. Chem. Phys.* **1984**, *81*, 4906−4914.
(21) Stöhr, J.; Sette, F.; Johnson, A. L. Near-Edge X-ray Absorption Fine-Structure Studies of Chemisorbed Hydrocarbons: Bond Lengths with a Ruler. *Phys. Rev. Lett.* **1984**, *53*, 1684−1687.
(22) Stevens, J. S.; Gainar, A.; Suljoti, E.; Xiao, J.; Golnak, R.; Aziz, E. F.; Schroeder, S. L. M. Chemical Speciation and Bond Lengths of Organic Solutes by Core Level Spectroscopy: pH- and Solvent-Influence on p-Aminobenzoic Acid. *Chem. - Eur. J.* **2015**, *21*, 7256−7263.
(23) Piancastelli, M. N. The Neverending Story of Shape Resonances. *J. Electron Spectrosc. Relat. Phenom.* **1999**, *100*, 167−190.
(24) Hitchcock, A. P.; Brion, C. E. K-Shell Excitation of HF and F_2 Studied by Electron Energy-Loss Spectroscopy. *J. Phys. B: At. Mol. Phys.* **1981**, *14*, 4399−4413.
(25) Arvanitis, D.; Haack, N.; Ceballos, G.; Wende, H.; Baberschke, K.; Ankudinov, A. L.; Rehr, J. J. Shape Resonances of Oriented Molecules. *J. Electron Spectrosc. Relat. Phenom.* **2000**, *113*, 57−65.
(26) Piancastelli, M. N.; Lindle, D. W.; Ferrett, T. A.; Shirley, D. A. The Relationship Between Shape Resonances and Bond Lengths - Reply. *J. Chem. Phys.* **1987**, *87*, 3255−3256.
(27) Piancastelli, M. N.; Lindle, D. W.; Ferrett, T. A.; Shirley, D. A. The Relationship Between Shape Resonances and Bond Lengths. *J. Chem. Phys.* **1987**, *86*, 2765−2771.
(28) Kempgens, B.; Köppe, H. M.; Kivimäki, A.; Neeb, M.; Maier, K.; Hergenhahn, U.; Bradshaw, A. M. Reappraisal of the Existence of Shape Resonances in the Series C_2H_2, C_2H_4, and C_2H_6. *Phys. Rev. Lett.* **1997**, *79*, 35−38.
(29) Kempgens, B.; Köppe, H. M.; Kivimäki, A.; Neeb, M.; Maier, K.; Hergenhahn, U.; Bradshaw, A. M. On the Correct Identification of Shape Resonances in NEXAFS. *Surf. Sci.* **1999**, *425*, L376−L380.
(30) Haack, N.; Ceballos, G.; Wende, H.; Baberschke, K.; Arvanitis, D.; Ankudinov, A. L.; Rehr, J. J. Shape Resonances of Oriented Molecules: ab initio Theory and Experiment on Hydrocarbon Molecules. *Phys. Rev. Lett.* **2000**, *84*, 614−617.
(31) Shneerson, V. L.; Saldin, D. K.; Tysoe, W. T. On the Dependence with Bond Lengths of the Observed Energies of NEXAFS Resonances of Diatomic Molecules. *Surf. Sci.* **1997**, *375*, 340−352.
(32) Hardie, A. G.; Dynes, J. J.; Kozak, L. M.; Huang, P. M. The Role of Glucose in Abiotic Humification Pathways as Catalyzed by Birnessite. *J. Mol. Catal. A: Chem.* **2009**, *308*, 114−126.
(33) Solomon, D.; Lehmann, J.; Kinyangi, J.; Liang, B.; Heymann, K.; Dathe, L.; Hanley, K.; Wirick, S.; Jacobsen, C. Carbon (1s) NEXAFS Spectroscopy of Biogeochemically Relevant Reference Organic Compounds. *Soil Sci. Soc. Am. J.* **2009**, *73*, 1817−1830.
(34) Dietrich, P. M.; Horlacher, T.; Girard-Lauriault, P. L.; Gross, T.; Lippitz, A.; Min, H.; Wirth, T.; Castelli, R.; Seeberger, P. H.; Unger, W. E. S. Adlayers of Dimannoside Thiols on Gold: Surface Chemical Analysis. *Langmuir* **2011**, *27*, 4808−4815.
(35) Schroeder, S. L. M.; Moggridge, G. D.; Ormerod, R. M.; Rayment, T.; Lambert, R. M. What Determines the Probing Depth of Electron Yield XAS? *Surf. Sci.* **1995**, *324*, L371−L377.
(36) Schroeder, S. L. M. Towards a 'Universal Curve' for Total Electron-Yield XAS. *Solid State Commun.* **1996**, *98*, 405−409.
(37) Schroeder, S. L. M. Probing Depth of Total Electron-Yield XAFS: Monte-Carlo Simulations of Auger Electron Trajectories. *J. Phys. IV* **1997**, *7*, C2-153−C2-154.
(38) Schroeder, S. L. M.; Moggridge, G. D.; Lambert, R. M.; Rayment, T. Electron-Yield X-ray Absorption Spectroscopy in Gaseous Environments. In *Spectroscopy for Surface Science*; Advances in Spectroscopy; Clark, R. J. H., Hester, R. E., Eds.; Wiley & Sons: New York, Chichester, 1998; Vol. *26*, pp 1−70.
(39) Sohn, K. E.; Dimitriou, M. D.; Genzer, J.; Fischer, D. A.; Hawker, C. J.; Kramer, E. J. Determination of the Electron Escape Depth for NEXAFS Spectroscopy. *Langmuir* **2009**, *25*, 6341−6348.
(40) Frazer, B. H.; Gilbert, B.; Sonderegger, B. R.; De Stasio, G. The probing depth of total electron yield in the sub-keV range: TEY-XAS and X-PEEM. *Surf. Sci.* **2003**, *537*, 161−167.
(41) Tanuma, S.; Powell, C. J.; Penn, D. R. Calculations of Electron Inelastic Mean Free Paths 0.5. Data for 14 Organic-Compounds Over the 50−2000 Ev Range. *Surf. Interface Anal.* **1994**, *21*, 165−176.
(42) Ravel, B.; Newville, M. ATHENA, ARTEMIS, HEPHAESTUS: Data Analysis for X-ray Absorption Spectroscopy Using IFEFFIT. *J. Synchrotron Radiat.* **2005**, *12*, 537−541.
(43) Ravel, B.; Newville, M. ATHENA and ARTEMIS: Interactive Graphical Data Analysis Using IFEFFIT. *Phys. Scr.* **2005**, *T115*, 1007−1010.
(44) Kanters, J. A.; Roelofsen, G.; Alblas, B. P.; Meinders, I. Crystal and Molecular-Structure of β-D-Fructose, with Emphasis on Anomeric Effect and Hydrogen-Bond Interactions. *Acta Crystallogr., Sect. B: Struct. Crystallogr. Cryst. Chem.* **1977**, *33*, 665−672.
(45) Mostad, A. X-ray Crystallographic Study of alpha-Glucose at 140 K. *Acta Chem. Scand.* **1994**, *48*, 276−278.
(46) Ohanessian, J.; Gillier-Pandraud, H. Structure Cristalline de l'α-D-Galactose. *Acta Crystallogr., Sect. B: Struct. Crystallogr. Cryst. Chem.* **1976**, *32*, 2810−2813.
(47) Hordvik, A. The Crystal and Molecular Structure of alpha-Xylose. *Acta Chem. Scand.* **1971**, *25*, 2175−2182.
(48) Gress, M. E.; Jeffrey, G. A. A Neutron Diffraction Refinement of Crystal Structure of β-Maltose Monohydrate. *Acta Crystallogr., Sect. B: Struct. Crystallogr. Cryst. Chem.* **1977**, *33*, 2490−2495.
(49) Noordik, J. H.; Beurskens, P. T.; Bennema, P.; Visser, R. A.; Gould, R. O. Crystal-Structure, Polarity and Morphology of 4-O-β-D-Galactopyranosyl-α-D-Glucopyranose Monohydrate (α-Lactose Monohydrate): a Redetermination. *Z. Kristallogr.* **1984**, *168*, 59−65.

DOI: 10.1021/acs.jpcb.5b07159
J. Phys. Chem. B 2015, 119, 14373−14381

(50) Ankudinov, A. L.; Conradson, S. D.; de Leon, J. M.; Rehr, J. J. Relativistic XANES Calculations of Pu Hydrates. *Phys. Rev. B: Condens. Matter Mater. Phys.* **1998**, *57*, 7518−7525.
(51) Battle, G. M.; Ferrence, G. M.; Allen, F. H. Applications of the Cambridge Structural Database in Chemical Education. *J. Appl. Crystallogr.* **2010**, *43*, 1208−1223.
(52) Nishiyama, Y.; Sugiyama, J.; Chanzy, H.; Langan, P. Crystal Structure and Hydrogen Bonding System in Cellulose I(alpha) from Synchrotron X-ray and Neutron Fiber Diffraction. *J. Am. Chem. Soc.* **2003**, *125*, 14300−14306.
(53) Garnier, S.; Petit, S.; Coquerel, G. Dehydration Mechanism and Crystallisation Behaviour of Lactose. *J. Therm. Anal. Calorim.* **2002**, *68*, 489−502.
(54) Jeffrey, G. A. Intramolecular Hydrogen-Bonding in Carbohydrate Crystal-Structures. *Carbohydr. Res.* **1973**, *28*, 233−241.

DOI: 10.1021/acs.jpcb.5b07159
J. Phys. Chem. B 2015, 119, 14373−14381